AGU PUBLICATIONS

Geochemistry, Geophysics, Geosystems

RESEARCH ARTICLE
10.1002/2016GC006434

Special Section:
FRONTIERS IN GEOSYSTEMS: Deep Earth - surface interactions

Large fluctuations of shallow seas in low-lying Southeast Asia driven by mantle flow

Sabin Zahirovic[1], Nicolas Flament[1], R. Dietmar Müller[1], Maria Seton[1], and Michael Gurnis[2]

[1]EarthByte Group, School of Geosciences, University of Sydney, Sydney, New South Wales, Australia, [2]Seismological Laboratory, California Institute of Technology, Pasadena, California, USA

Key Points:
- Late Cretaceous-Eocene regional unconformity in Southeast Asia likely driven by dynamic topography
- Collision of Gondwana-derived terranes choked subduction and resulted in regional dynamic uplift
- Linked tectonic and mantle flow models highlight influence of plate-mantle system on surface processes

Supporting Information:
- Supporting Information S1
- Supporting Information S2
- Movie S1
- Movie S2
- Movie S3

Correspondence to:
S. Zahirovic,
sabin.zahirovic@sydney.edu.au

Citation:
Zahirovic, S., N. Flament, R. Dietmar Müller, M. Seton, and M. Gurnis (2016), Large fluctuations of shallow seas in low-lying Southeast Asia driven by mantle flow, *Geochem. Geophys. Geosyst.*, *17*, 3589–3607, doi:10.1002/2016GC006434.

Received 9 MAY 2016
Accepted 10 AUG 2016
Accepted article online 12 AUG 2016
Published online 13 SEP 2016

Abstract The Sundaland continental promontory, as the core of Southeast Asia, is one of the lowest lying continental regions, with half of the continental area presently inundated by a shallow sea. The role of mantle convection in driving long-wavelength topography and vertical motion of the lithosphere in this region has often been ignored when interpreting regional stratigraphy, including a widespread Late Cretaceous-Eocene unconformity, despite a consensus that Southeast Asia is presently situated over a large-amplitude dynamic topography low resulting from long-term post-Pangea subduction. We use forward numerical models to link mantle flow with surface tectonics and compare predicted trends of dynamic topography with eustasy and regional paleogeography to determine the influence of mantle convection on regional basin histories. A Late Cretaceous collision of Gondwana-derived terranes with Sundaland choked the active margin, leading to slab breakoff and a ~10–15 Myr-long subduction hiatus. A subduction hiatus likely resulted in several hundred meters of dynamic uplift and emergence of Sundaland between ~80 and 60 Ma and may explain the absence of a Late Cretaceous-Eocene sedimentary record. Renewed subduction from ~60 Ma reinitiated dynamic subsidence of Sundaland, leading to submergence from ~40 Ma despite falling long-term global sea levels. Our results highlight a complete "down-up-down" dynamic topography cycle experienced by Sundaland, with transient dynamic topography manifesting as a major regional unconformity in sedimentary basins.

1. Introduction

The Indonesian islands and surrounding region represent one of the most low-lying continental areas on Earth with almost half of this region, known as Sundaland, presently inundated by a shallow sea (Figure 1a). The present-day low-regional elevation has been attributed to the massive volume of oceanic slabs sinking in the mantle beneath Southeast Asia, leading to regional dynamic subsidence [*Bertelloni and Gurnis*, 1997; *Spasojevic and Gurnis*, 2012]. However, a Late Cretaceous to Eocene regional unconformity [*Clements et al.*, 2011; *Doust and Sumner*, 2007] indicates that shallow seas retreated following regional flooding during the mid-Cretaceous (Figure 1b) sea level highstand [*Haq*, 2014; *Haq et al.*, 1987]. During the Eocene, less than one fifth of Sundaland was submerged (Figure 1c), despite estimates of global sea level being ~200 m higher than at present [*Haq and Al-Qahtani*, 2005; *Haq et al.*, 1987]. Here we use forward models in combination with regional paleogeography and estimates of eustasy to unravel how plate tectonics and mantle convection may have influenced the flooding of Sundaland through time.

The post-Pangea tectonic history of Sundaland is dominated by long-lived subduction of oceanic plates, including the Tethyan ocean basins from the south, and the Izanagi and Pacific oceanic plates from the east [*Hutchison*, 1975; *Katili*, 1975; *Metcalfe*, 1988; *Seton et al.*, 2012]. The initiation of subduction along southern Eurasia during the Late Jurassic is suggested to have resulted in dynamic subsidence and the deposition of widespread Late Jurassic-Early Cretaceous red beds (Figure 2) across Sundaland [*Clements et al.*, 2011]. Independently, mid-Cretaceous greenhouse conditions and a seafloor spreading pulse that produced large areas of young buoyant oceanic seafloor resulted in rising global sea levels [*Seton et al.*, 2009], reflected in a number of eustatic sea level curves [*Haq*, 2014; *Haq and Al-Qahtani*, 2005; *Haq et al.*, 1987; *Müller et al.*, 2008]. A regional paleogeographic reconstruction [*Golonka et al.*, 2006] suggests that flooding of Sundaland peaked in mid-Cretaceous times between ~120 and 90 Ma (Figure 1b), coincident with rising global sea levels and dynamic subsidence from a well-established subduction zone along the Sundaland margin, leading to the advance of shallow seas on the Sunda Shelf.

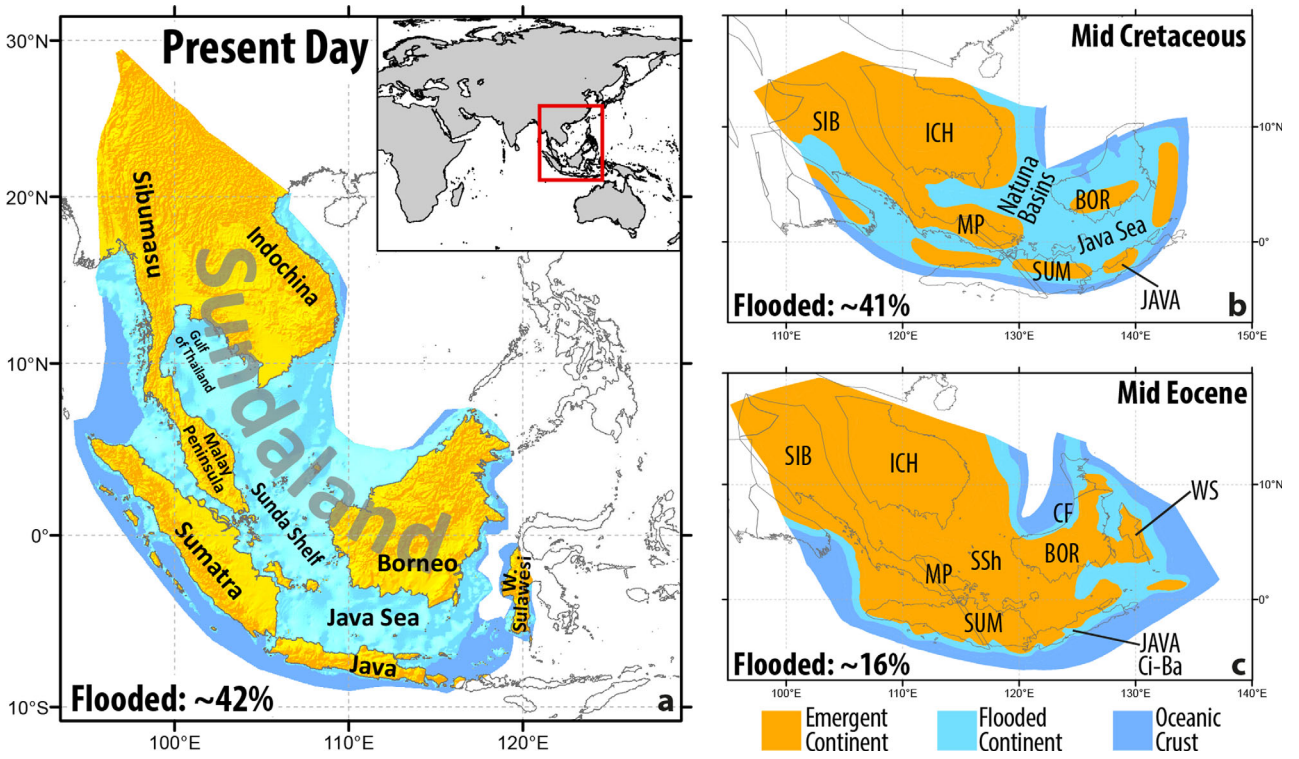

Figure 1. Long-term continental inundation of Sundaland. (a) About 42% of Sundaland continental area is flooded at present, which is similar to (b) the mid-Cretaceous. In contrast, the continental promontory was emergent for much of the Eocene (c), a period marked by erosional environments corresponding to a widespread regional unconformity [*Clements et al.*, 2011]. Past inundation patterns were deduced from paleogeographic reconstructions of *Golonka et al.* [2006]. Oceanic crust (dark blue) is not included in the calculation of inundation. BOR, Borneo (Schwaner Core); CF, Crocker Fan; Ci–Ba, Ciemas and Bayah Formations; ICH, Indochina; MP, Malay Peninsula; SIB, Sibumasu; SSh, Sunda Shelf; SUM, Sumatra; WS, West Sulawesi.

The East Java and West Sulawesi continental fragments were approaching the Sundaland active margin in the Late Cretaceous, with the lack of volcanic-derived zircons after 80 Ma [*Clements and Hall*, 2011] suggesting the end of subduction in this segment of the margin and suturing of these terranes to the core of Sundaland. Further west, subduction ceased on the Sumatra margin by ~75 Ma as a result of Woyla back-arc closure and intraoceanic terrane accretion onto Sundaland [*Zahirovic et al.*, 2014]. This timing is consistent with a magmatic gap between ~75 and 60 Ma on Sumatra, suggesting a ~10–15 Myr hiatus in subduction along this margin [*McCourt et al.*, 1996]. These suturing events interrupted subduction along southern Sundaland and could have induced slab break-off, as has been suggested following continental collisions [*Davies and von Blanckenburg*, 1995; *Duretz et al.*, 2014]. Computations in a three-dimensional domain by *van Hunen and Allen* [2011] suggest that slab break-off may occur 10–20 Myr after the entry of continental crust into a subduction zone, while the computations of *Li et al.* [2013], also in 3-D, highlight the complexity and diachroneity of slab tearing following collision. Since we impose a hiatus in subduction between ~75 and 60 Ma, our method does not capture the geodynamic complexity of slab breakoff (see Methods). However, our approach allows us to investigate the consequences of a subduction hiatus on the large-scale topography of the overriding plate.

Dynamic uplift following slab detachment is thought to be responsible for the widespread emergence of Sundaland and the establishment of erosional regimes from Late Cretaceous to Eocene times, resulting in a regional unconformity across Sundaland [*Clements et al.*, 2011; *Doust and Sumner*, 2007] (Figure 3). Large volumes of sediment were transported beyond the continental slope of the Sunda Shelf (Figure 2)—including sediment shed into the accretionary prisms of northern Borneo and southern Java [*Clements and Hall*, 2007]. Importantly, Late Cretaceous to Eocene sediments are missing from almost all Sundaland basins [*Clements et al.*, 2011; *Doust and Sumner*, 2007] (Figure 3), and thus the crustal deformation and uplift caused by Late Cretaceous collisions of continental blocks to southern Sundaland are unlikely to be the dominant mechanism responsible for the regional nature of the unconformity. Lithospheric flexure in response to loading by orogenic belts generally results in downwarping inboard

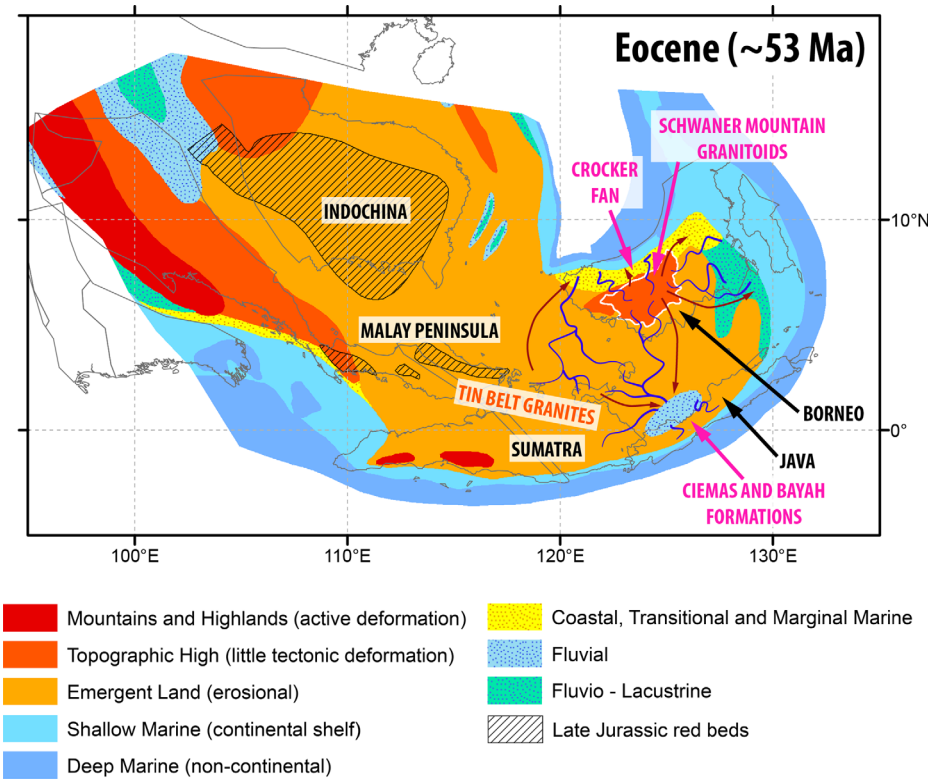

Figure 2. Eocene paleogeographic reconstruction, modified from *Golonka et al.* [2006] and *Clements and Hall* [2011], highlighting the likely sources of sediments (Tin Belt Granites, Schwaner Mountain Granitoids, etc.) and the likely sediment sinks (Crocker Fan, Java basins, and accretionary prism) from sedimentary provenance studies. Late Jurassic to Early Cretaceous red beds are plotted from *Clements et al.* [2011]. Inferred paleo-drainage patterns (dark blue lines) for the Eocene are shown only for schematic purposes. Brown arrows indicate the likely sedimentary provenance across Sundaland.

of the active continental margin, and the establishment of foreland basins. This would lead to localized flooding in the vicinity of the subduction zone, but not over large continent-wide spatial scales. Moreover, flexural deformation and crustal deformation are typically limited to spatial scales of ~100–200 km [*Buiter et al.*, 2002; *Gurnis*, 1991; *McKenzie*, 2010], whereas wavelengths of mantle-driven topography are typically many hundreds or thousands of kilometers, depending on the depth of density anomalies [*Hager et al.*, 1985].

Although the long-wavelength dynamic uplift of Sundaland resulting from slab breakoff has been proposed conceptually [*Clements et al.*, 2011], here we explicitly test such a scenario in the context of plate tectonics, geodynamics, paleogeography, and the role of long-term changing sea levels in modifying the long-term flooding and emergence of Sundaland. We use 4-D (3-D space and time) global mantle flow numerical models [*Bower et al.*, 2015; *Flament et al.*, 2014] coupled with regionally refined global plate reconstructions [*Zahirovic et al.*, 2014] to investigate the space-time evolution of dynamic topography associated with the history of slab breakoff and subduction reinitiation, and the response of the overriding Sundaland continent.

2. Methods

2.1. Flooding Extent From Paleogeographic Reconstructions

Paleogeographic maps that are constructed from detailed regional syntheses of paleo-facies distributions provide a powerful insight into the shifting depositional (and erosional) environments deep in geological time. A detailed paleogeographic map for Borneo and Sulawesi exists only for the Cenozoic [*Wilson and Moss*, 1999], but not for the rest of Sundaland back to the Cretaceous. A synthesis of basin sedimentary histories across Southeast Asia [*Doust and Sumner*, 2007] provides a deeper time and wider spatial context for depositional regions (Figures 3 and 4). The paleogeographic maps of *Golonka et al.* [2006] are paleo-environmental reconstructions for both erosional and depositional regions, in a plate tectonic context for

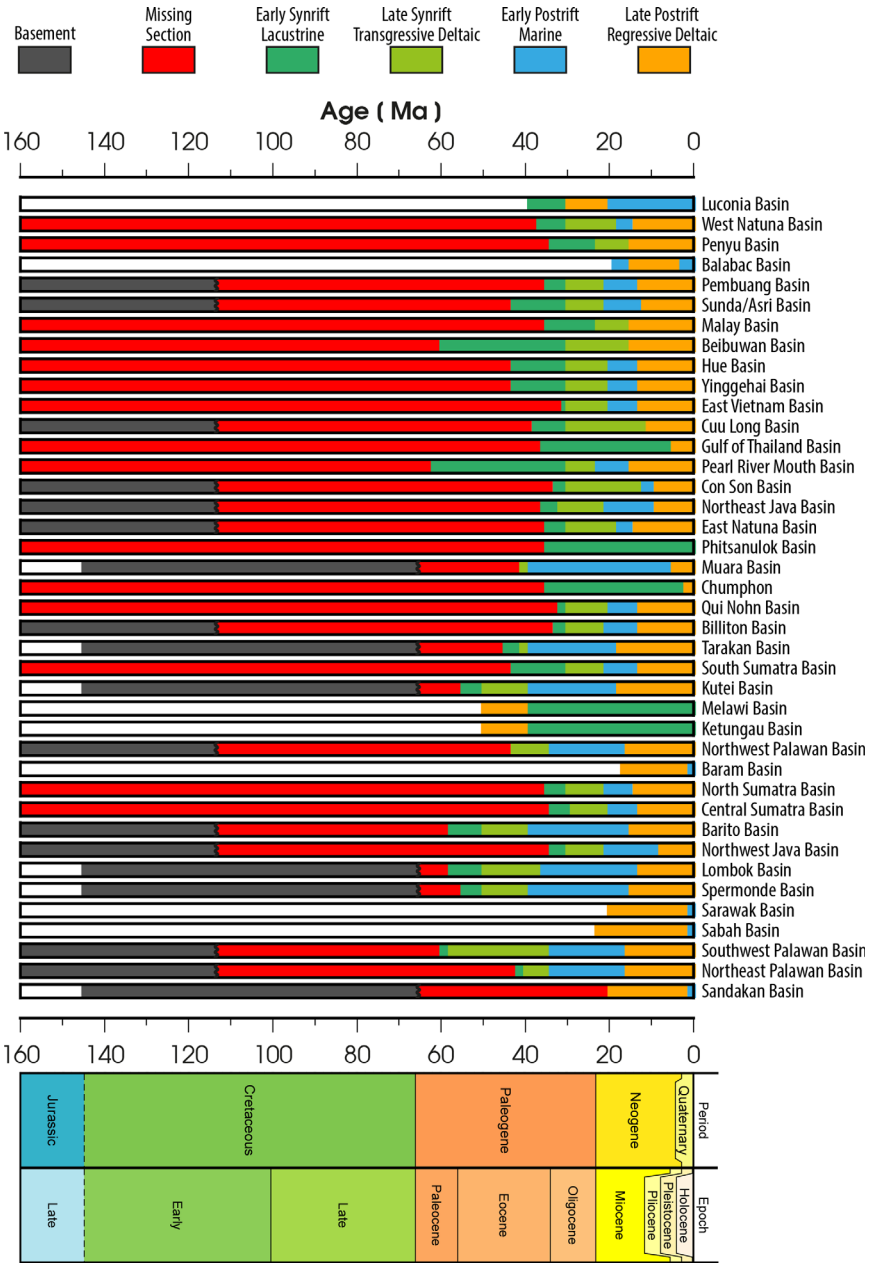

Figure 3. Simplified schematic of basin histories for Southeast Asia synthesized from *Doust and Sumner* [2007], including the changing tectonic and paleo-environmental settings recorded in the sedimentary sequences. The regional unconformity across Sundaland was extracted from each basin (red), highlighting the dominance of Late Cretaceous to Eocene erosional environments on Sundaland. The advance of shallow seas on Sundaland is recorded as the progression from lacustrine environments during ~45–30 Ma to transgressive deltaic settings during ~30–22 Ma, followed by fully marine environments until ~15 Ma. However, by ~15 Ma global sea levels had fallen significantly due to growing inland ice sheets where long-term advance of flooding of Sundaland was likely reversed. Full long-term exposure of Sundaland, as experienced in the latest Cretaceous to Paleocene, has not occurred since ~15 Ma as demonstrated by continued deposition of regressive deltaic sequences. Wavy lines represent unconformable contacts, many of which have age uncertainties. Basin names and outlines are provided in Figure S1.

the entire Southeast Asia region (Figure S2), that span our model timeframe, as well as the entire Phanerozoic. We georeferenced paleogeographic reconstructions of Southeast Asia from *Golonka et al.* [2006] to an equivalent relative plate motion model [*Wright et al.*, 2013] and converted paleo-environments to categories of oceanic crust, inundated continental crust, and emergent continental crust (Figure 5). For the purpose of calculating areas of inundation and emergence, the polygons representing the paleogeographies were reprojected into an equal-area cylindrical coordinate system with a central meridian of 110°E and a

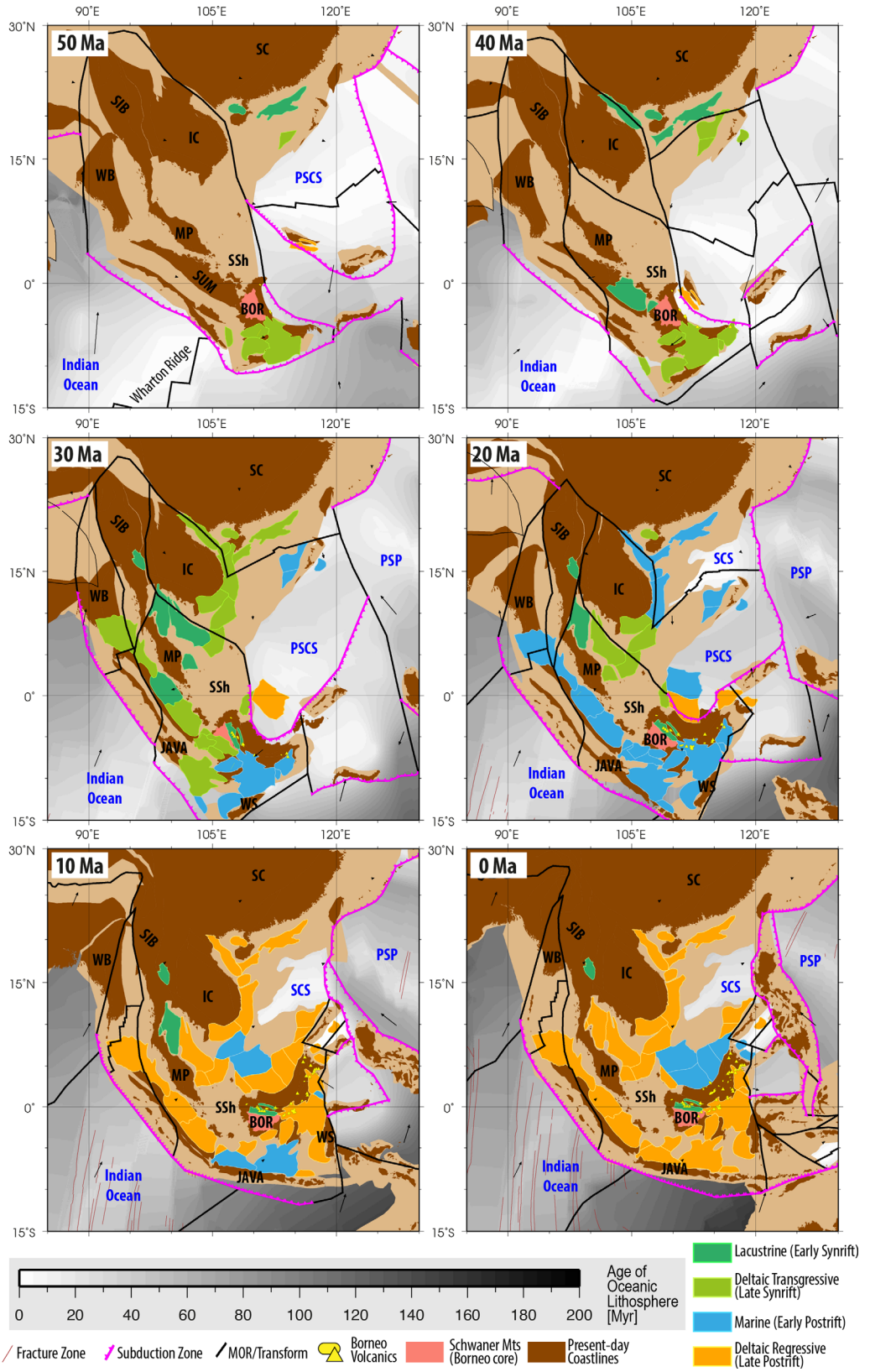

Figure 4. Paleo-environments interpreted from basin stratigraphy as age-coded from *Doust and Sumner* [2007], attached to the plate reconstruction of *Zahirovic et al.* [2014], show progressive flooding and sedimentary deposition in Sundaland basins since the Eocene. Plate boundaries and velocities are presented as well as seafloor ages in shades of grey. IC = Indochina, SC = South China, BOR = Borneo, WS = West Sulawesi, WB = West Burma, MP = Malay Peninsula, SIB = Sibumasu, SSh = Sunda Shelf, (P)SCS = (Proto) South China Sea, PSP = Philippine Sea Plate.

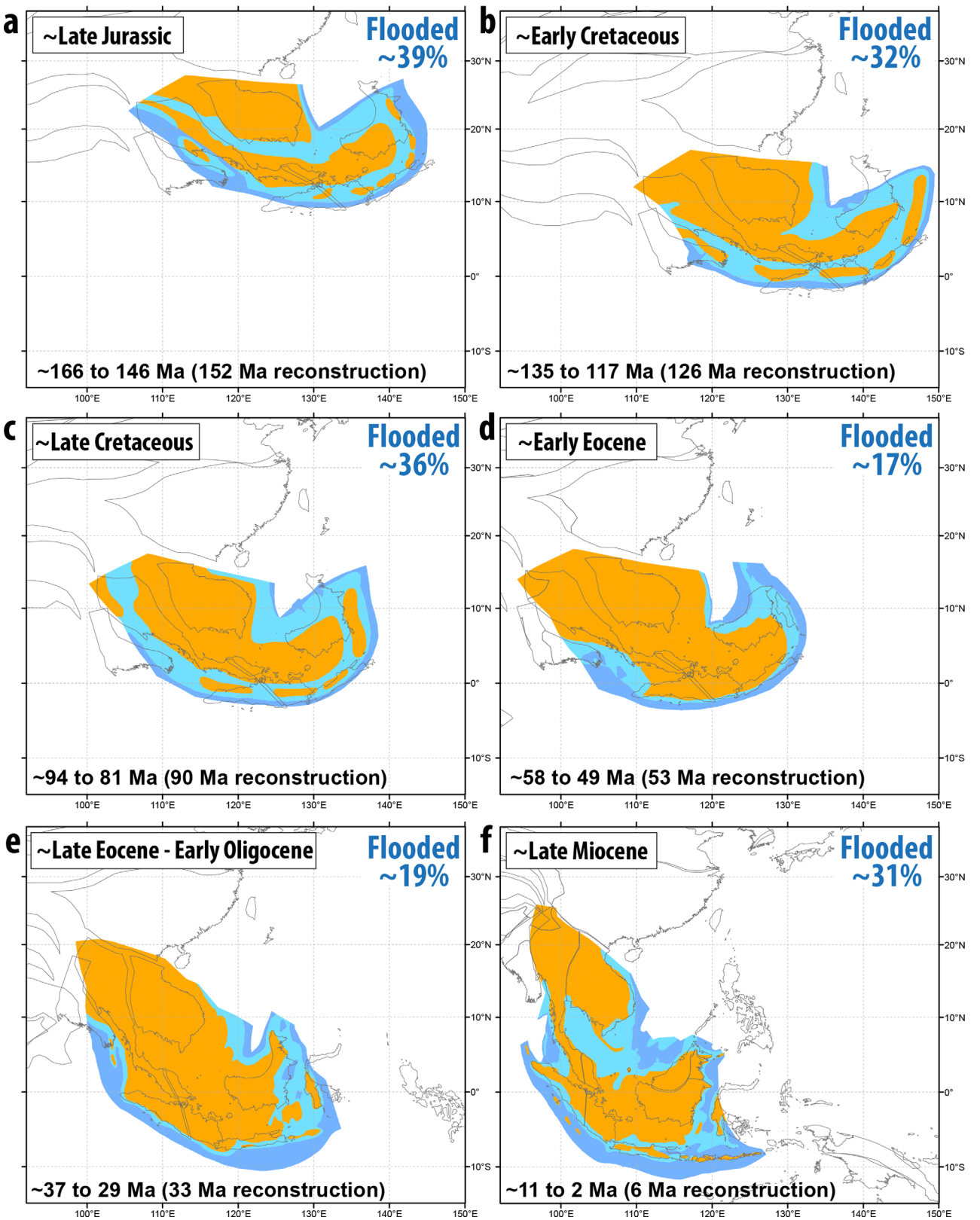

Figure 5. Long-term continental inundation of Sundaland derived from *Golonka et al.* [2006]. Inundated continental areas (light blue) are most widespread in the Late Jurassic, Cretaceous and post-Miocene times. Conversely, much of the continental area is emergent (orange) by Eocene times, consistent with the widespread erosional/non-depositional regime on Sundaland that represents the regional Late Cretaceous-Eocene unconformity [*Clements et al.*, 2011]. Post-Eocene flooding propagated into the Sunda Shelf and the Gulf of Thailand, even though long-term eustatic sea levels were falling during this time [*Haq and Al-Qahtani*, 2005; *Haq et al.*, 1987]. The input paleogeographic maps are provided in Figure S2.

standard parallel of 0°N, suitable for the near-equatorial positions of Sundaland since the Jurassic. Paleogeographic snapshots in geological stages with ~10–20 Myr temporal intervals are informative for the long-term geography of Sundaland, and appropriate for comparisons with long-term sea level trends and topography evolution.

We calculated the long-term flooding of Sundaland from the area of inundated continental crust in the paleogeographic reconstructions (Figure 5). The extent of Sundaland includes Indochina, Sibumasu, the Malay Peninsula, Sumatra, and Borneo that have existed as a welded continental block since the Jurassic, albeit with tectonically reactivated boundaries following the propagating effects of the India-Eurasia collision [*Hall*, 2002; *Lee and Lawver*, 1995]. The continental portions of East Java and West Sulawesi were added following their accretion to Sundaland by ~80 Ma, as well as the accretion of Woyla arc material to Sumatra by ~75 Ma [*Zahirovic et al.*, 2014].

2.2. Plate Tectonics and Geodynamics of Sundaland

We model global mantle flow based on the subduction history predicted by a global tectonic reconstruction [*Seton et al.*, 2012] with refinements for Southeast Asia [*Zahirovic et al.*, 2014] that are embedded in a recent global synthesis [*Müller et al.*, 2016] (see Supporting Information). Viscous mantle flow is computed using

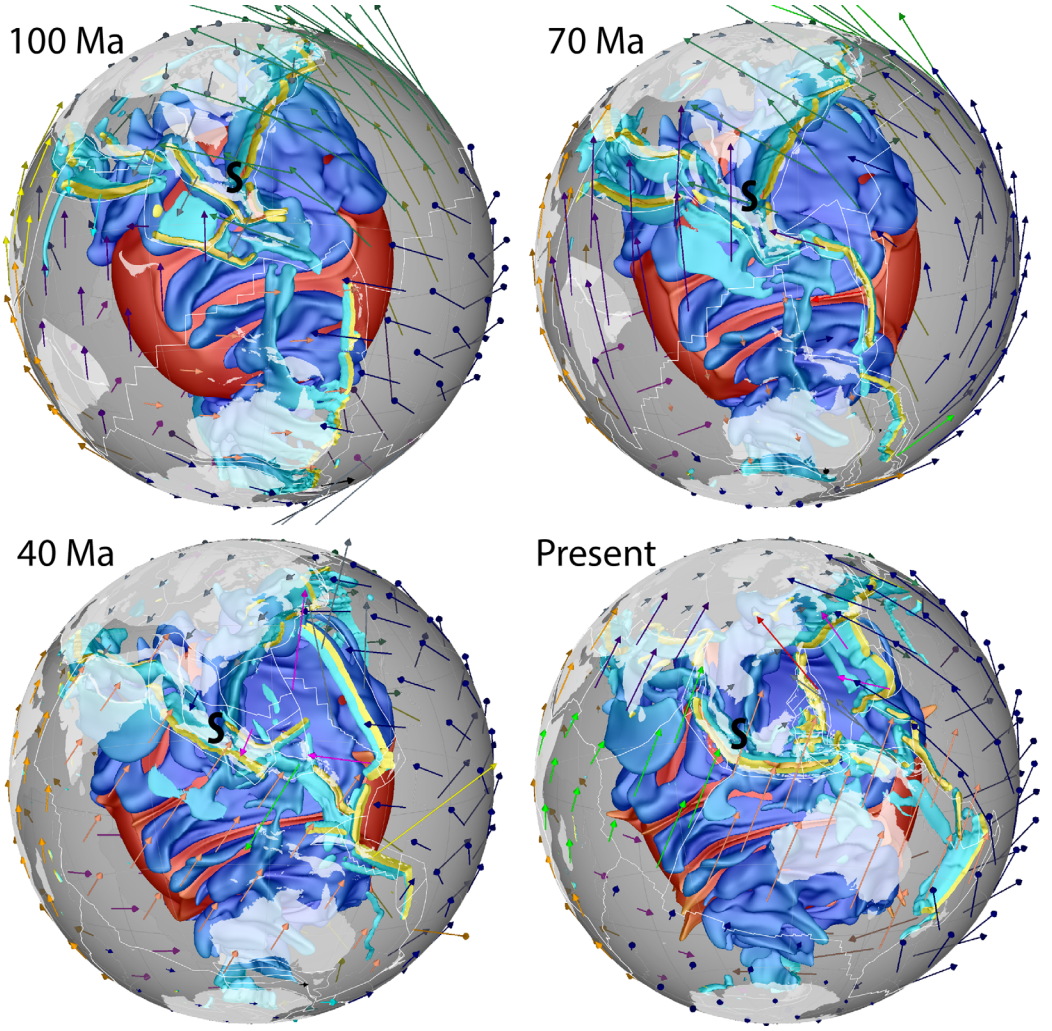

Figure 6. The large-scale mantle evolution from a 4-D global numerical model of mantle flow using CitcomS and visualized in GPlates. Time-dependent evolution of mantle flow coupled to the plate reconstructions for Case 4, with subducting lithosphere (blue), and large-scale mantle upwelling (red). The location of plate boundaries are plotted as white lines, subduction zones are thick yellow regions, plate velocities are colored vectors and reconstructed present-day coastlines as white translucent regions centered on Sundaland (S). See Animation S2.

Table 1. Parameters Common to All Model Cases[a]

Parameter	Symbol	Value	Units
Rayleigh number	Ra	7.84×10^7	
Thermal expansion coefficient	α_0	3×10^{-5}	K^{-1}
Density	ρ_0	4000	kg m^{-3}
Gravity acceleration	g_0	9.81	m s^{-2}
Temperature change	ΔT	2825	K
Temperature offset	T_η	452	K
Background mantle temperature	T_b	1685	K
Mantle thickness	h_M	2867	km
Earth radius	R_0	6371	km
Universal gas constant	R	8.31	J mol^{-1} K^{-1}
Thermal diffusivity	κ_0	1×10^{-6}	m^2 s^{-1}
Reference viscosity	η_0	1×10^{21}	Pa s
Activation energy (upper mantle)	$E_{\eta UM}$	100	kJ mol^{-1}
Activation energy (lower mantle)	$E_{\eta LM}$	33	kJ mol^{-1}
Activation temperature	T_η	452	K

[a]Subscript "0" denotes reference values.

CitcomS [*Zhong et al*., 2008] and is driven by plate velocities (Figure 6) applied as time-dependent boundary conditions while the thermal structure of lithosphere and slabs are progressively assimilated in 1 Myr intervals from the plate reconstructions following *Bower et al*. [2015].

In the initial condition at 230 Ma, a thermochemical layer 113 km thick at the base of the mantle is assumed, in which material is 3.6% denser than ambient mantle. This setup suppresses the formation of mantle plumes, which allows subduction-driven dynamic topography to be isolated [*Flament et al*., 2014]. The temperature and thickness of the lithosphere is derived using a half-space cooling model and the synthetic age of the ocean floor [*Bower et al*., 2015]. The global thermal structure of slabs is based on the location of subduction zones and on the age of the adjacent ocean floor [*Bower et al*., 2015]. In the initial condition, slabs are inserted down to 1400 km depth, with a dip of 45° down to 425 km depth and a dip of 90° below 425 km. Subduction zones thought to have initiated just prior to 230 Ma are inserted to a depth based on their subduction duration and assuming a descent rate of 3 and 1.2 cm/yr in the upper and lower mantle, respectively. Slabs are initially twice as thick in the lower mantle than in the upper mantle to account for advective thickening. Subduction zones that appear during the model run are progressively inserted in the upper mantle. The global thermal structure of the lithosphere and of subducting slabs is inserted in the dynamic models at 1 Myr increments, to a depth of up to 350 km at subduction zones [*Bower et al*., 2015].

The Rayleigh number is defined as

$$Ra = \frac{\alpha_0 \rho_0 g_0 \Delta T h_M^3}{\kappa_0 \eta_0}, \tag{1}$$

where α is the coefficient of thermal expansivity, ρ the density, g the acceleration of gravity, ΔT the temperature change across the mantle, h_M is the thickness of the mantle, κ the thermal diffusivity, η the viscosity, and the subscript "0" indicates reference values. Values are listed in Table 1.

The viscosity of the mantle depends on pressure and temperature (Figure 7) following:

$$\eta = \eta_0(r) \exp\left(\frac{E_\eta}{R(T+T_\eta)} - \frac{E_\eta}{R(T_b+T_\eta)}\right), \tag{2}$$

where $\eta_0(r)$ is a prefactor defined with respect to the reference viscosity η_0 for four layers: it is equal to 1 above 160 km, either to 1 (for cases without asthenosphere, see Table 2) or to 0.1 (for cases with an asthenosphere, see Table 2) between 160 and 310 km depth, to 1 between 310 and 660 km depth and either to 100 or linearly increasing from 10 to 100 in the lower mantle below 660 km depth (see Table 2). E_η is the activation energy (E_{UM} in the upper mantle and E_{LM} in the lower mantle), R is the universal gas constant, T is the dimensional temperature, T_η is a temperature offset, and T_b is the ambient mantle temperature (values are listed in Table 1). The average model resolution, obtained with $\sim 13 \times 10^6$ nodes and radial mesh refinement, is ~50 km × 50 km × 15 km at the surface, ~28 km × 28 km × 27 km at the core-mantle boundary (CMB), and ~40 km × 40 km × 100 km in the midmantle.

We present mantle evolution from the latest Jurassic (~160 Ma), from which time the plate reconstructions in *Zahirovic et al*. [2014] are regionally refined (Figures 6 and 8), and extract the average dynamic topography acting on Sundaland from the Late Cretaceous (100 Ma) to present. The dynamic topography h is obtained by scaling the total normal stress σ_{rr} on the top model surface following:

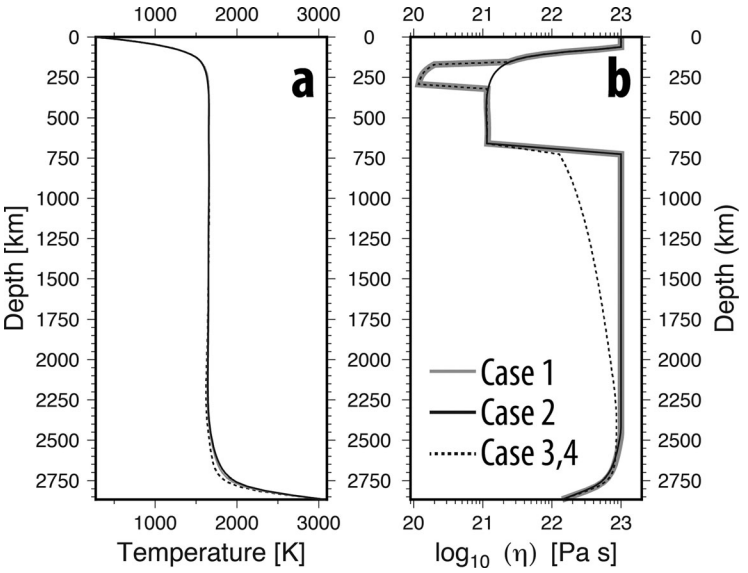

Figure 7. Horizontally averaged (a) temperature and (b) temperature-dependent viscosity radial profiles for Cases 1–4 at present day.

$$h = \frac{\sigma_{rr}}{\Delta\rho g_0}, \quad (3)$$

where $\Delta\rho$ is the density difference between the shallow mantle $\rho_{UM} = 3340$ kg m^{-3} and seawater ($\rho_w = 1030$ kg m^{-3}), R_0 is the radius of the Earth and other parameters are listed in Tables 1 and 2. Water-loaded dynamic topography is calculated from the vertical stress resulting from mantle flow in restarts of the main calculation with free-slip boundary conditions while ignoring buoyancy and lateral viscosity variations above 350 km depth, which is the maximum depth to which subducting slabs are inserted using time-dependent upper boundary conditions (see *Bower et al.* [2015] for details). As a result, we cannot model slab breakoff, and instead focus on the role of a subduction hiatus that we infer from a ~75–60 Ma magmatic gap on Sumatra. Four model cases were run to test the sensitivity of the results to the choice of radial viscosity profile and absolute plate motion model (Table 1 and Figure 7). Cases 1, 3, and 4 incorporate a low-viscosity asthenosphere, unlike Case 2. In Cases 3 and 4 we implement a progressive increase in viscosity from a factor of 10 at the base of the transition zone to a factor of 100 deeper in the lower mantle (10–100 in Table 2), following *Steinberger and Calderwood* [2006]. To test the influence of the absolute reference frame for plate motions, we apply the subduction-calibrated longitudinal positions from *van der Meer et al.* [2010] in Case 3, and a moving hot spot frame from *Torsvik et al.* [2008] and a True Polar Wander-corrected reference frame based on *Steinberger and Torsvik* [2008] for earlier times, as described in *Seton et al.* [2012] and *Müller et al.* [2016], for the other cases.

3. Results

3.1. Comparison of Present-Day Predictions to Residual Topography and Seismic Tomography

Predictions of present-day dynamic topography can be compared with estimates of residual topography taken from the synthesis of *Winterbourne et al.* [2014]. The dynamic topography for Southeast Asia is superimposed with point-estimates of residual topography (colored circles and triangles in Figure 9). A perfect fit between predicted dynamic topography and observed residual topography would result in a slope of 1, assuming that all or most of the residual topography is due to dynamic topography. Keeping in mind the scarcity of residual topography estimates, we assess which mantle viscosity and tectonic histories give the smaller RMS distance between predicted dynamic topography and residual topography.

Table 2. Parameters for Numerical Mantle Flow Models in Cases 1–4

	Case 1	Case 2	Case 3	Case 4
Mesh nodes	129 × 129 × 12 (nodes on the surface) × 65 (depth levels)			
Viscosity relative to reference viscosity (lithosphere, upper mantle/asthenosphere, transition zone, lower mantle)	1,0.1,1,100	1,1,1,100	1,0.1,1,10 → 100 following *Steinberger and Calderwood* [2006]	1,0.1,1,10 → 100
Plate reconstruction	*Zahirovic et al.* [2014]		Reconstructions from *Zahirovic et al.* [2014] with subduction-calibrated longitudinal positions from *van der Meer et al.* [2010]	*Zahirovic et al.* [2014]

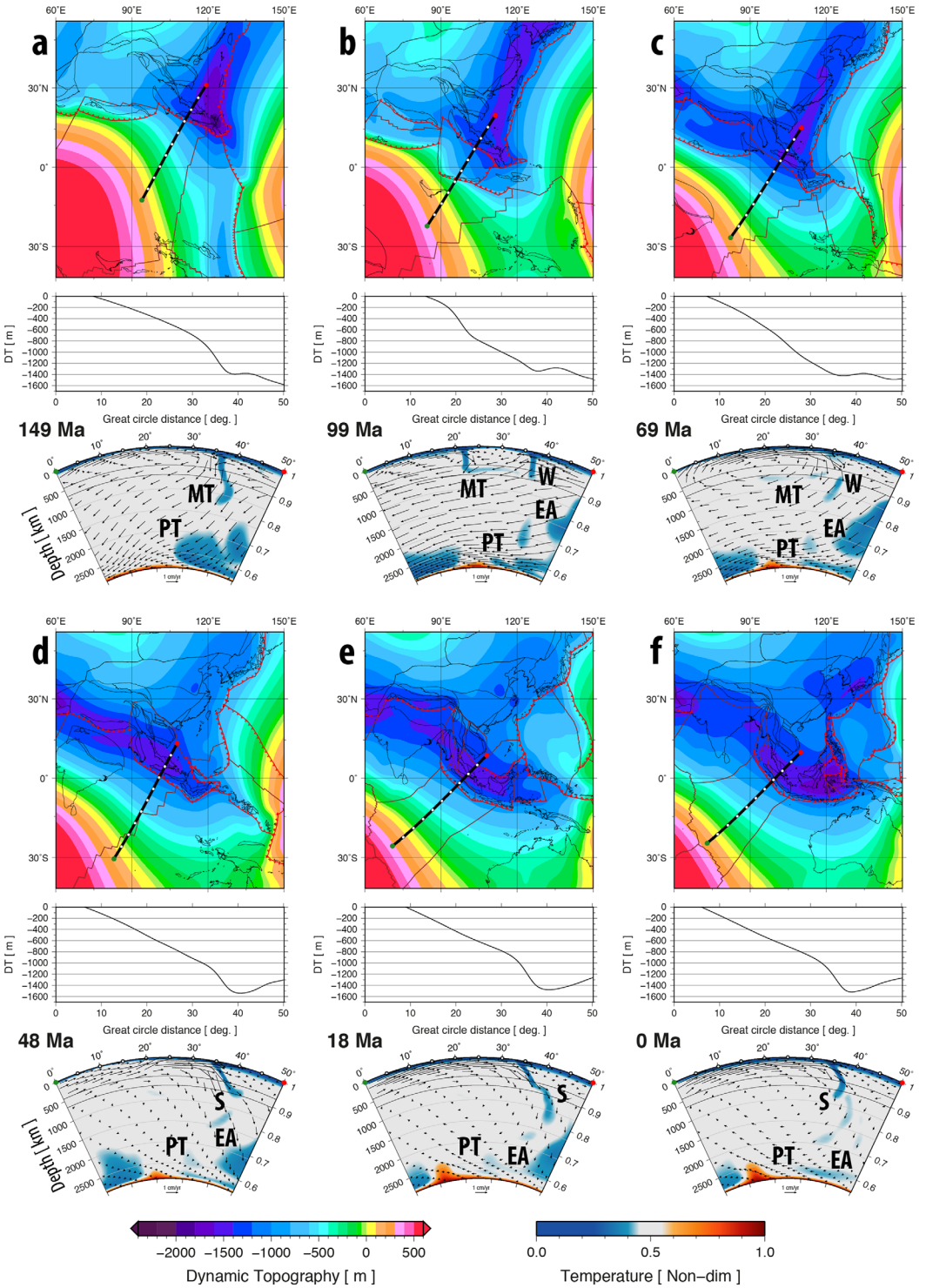

Figure 8. Model dynamic topography and temperature as predicted by Case 4. A great circle profile (thick black line) largely representative of the southern Sundaland active margin was reconstructed in the plate frame of reference (i.e., Sumatra fixed). The evolution of mantle temperature is represented on a vertical profile from the surface to the core-mantle boundary. The Early Cretaceous tectonics of Sundaland is dominated by the northward subduction of the Meso-Tethys (MT) and the southward subduction of Izanagi Plate along the Natuna and north Borneo active margins to produce the East Asian slabs (EA) that interact with Tethyan slabs at depth. Rollback and opening of the Woyla back-arc basin results in the formation of two independent Meso-Tethyan slabs, followed by the onset of Woyla back-arc basin subduction (W) by ~100 Ma. The accretion of West Sulawesi and East Java to Borneo by ~80 Ma interrupts subduction on eastern Sundaland, while the collision of the Woyla terranes with Sumatra from ~75 Ma obstructs subduction for ~10–15 Myr. Convergence and subduction is reestablished along the Sunda segment (S) at ~65–60 Ma, as indicated by the resumption of volcanism on Sumatra. The short-lived cessation of subduction results in dynamic uplift during the Late Cretaceous to Eocene, while dynamic subsidence resumes by ~40 Ma. PT, Paleo-Tethys slab. See Animation S3.

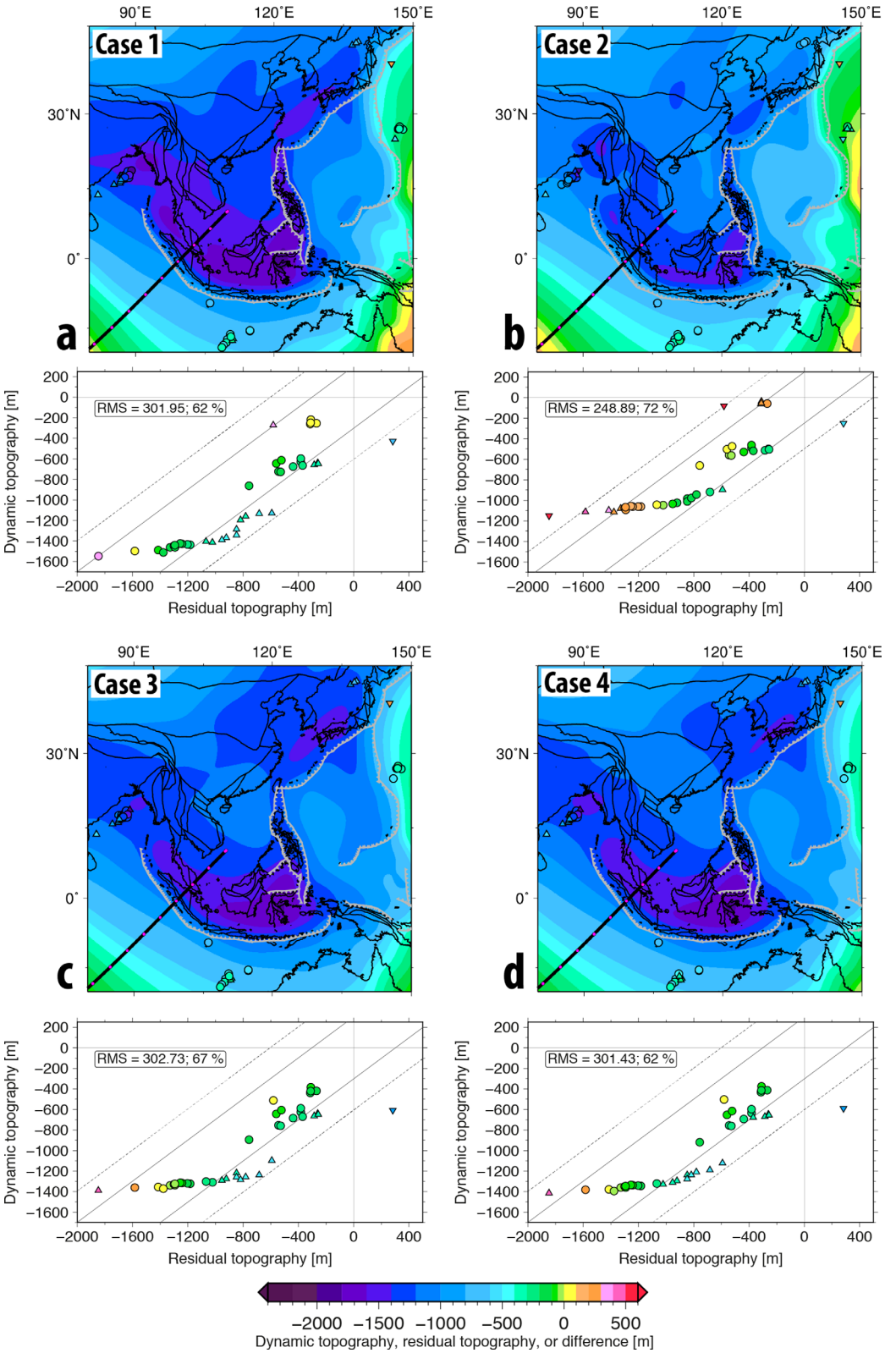

Figure 9. Present-day dynamic topography predicted by Cases 1–4 is plotted on the map in Figures 9a–9d, and superimposed with point estimates of residual topography from *Winterbourne et al.* [2014] (symbols colored according to residual topography). Root-mean-square (RMS) distance between predicted dynamic topography and the residual topography of *Winterbourne et al.* [2014] is presented in the scatterplots. Symbols are colored according to the difference between dynamic and residual topography. Circles are within one RMS, upward triangles are within two RMS, and inverted triangles are beyond two RMS.

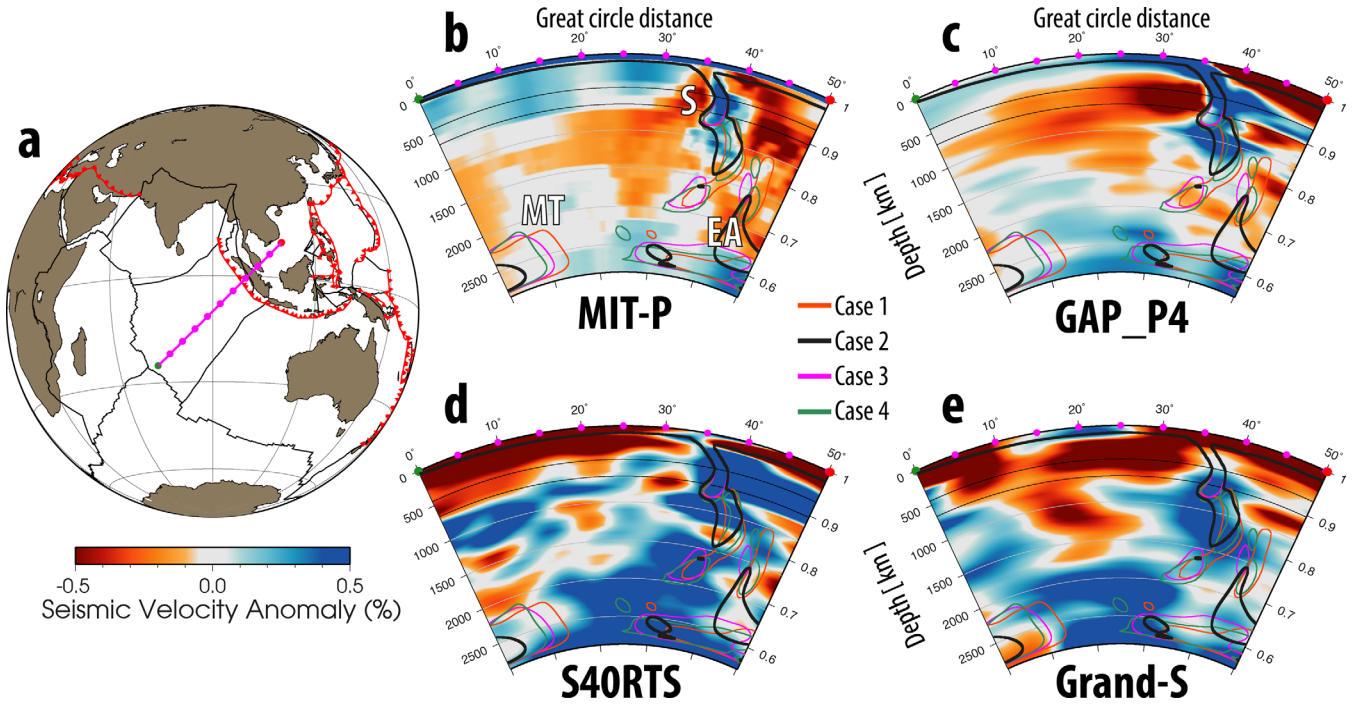

Figure 10. Comparison of model predictions with seismic tomography. The slab contours representing mantle 10% colder than ambient for Cases 1–4 along a present-day transect (a) are compared to Figures 10b–10e, equivalent vertical slices of *P* and *S* wave tomographic models [*Grand*, 2002; *Li et al.*, 2008; *Obayashi et al.*, 2013; *Ritsema et al.*, 2010]. The Sunda slab (S) is predicted by all models to a depth of ~1500 km, which is largely consistent with the tomographic models and earlier interpretations [*Widiyantoro and van der Hilst*, 1996]. Importantly, the seismic tomography models support the gap between the East Asian (EA) slabs in the lower mantle and the younger Sunda (S) slab in the mid to upper mantle predicted by all four mantle flow models, and are a manifestation of the ~80–65 Ma interruption of subduction along southern Sundaland. MT, Meso-Tethyan slabs. BF, Bengal Fan; SCS, South China Sea.

The present-day amplitude and spatial distribution of predicted dynamic topography across Southeast Asia are generally consistent with available constraints on residual topography [*Winterbourne et al.*, 2014], as reflected by a root-mean-square (RMS) distance of ~250–300 m between predictions (dynamic topography ranging between approximately −1600 and 0 m across all models) and constraints (residual topography ranging between approximately −1800 and +200 m). Assumptions underlying the estimates of residual topography by *Winterbourne et al.* [2014] used here include a model for the cooling of the oceanic lithosphere, and a model for the seismic velocity of sedimentary columns in the oceans. As with standard deviations, predicted versus observed values within one RMS error (Figure 9, gray lines) are assumed to represent a good fit and are plotted as circles. Acceptable values, within two RMS errors (Figure 9, dashed gray lines), are plotted as upright triangles. Between 62 and 72% of predictions fall within one RMS across model cases (Figure 9). One value in the Bengal Fan region (BF, Figure 9b), and one to two values in the Pacific (Figures 9a–9d) are outside the acceptable errors (plotted as inverted triangles). However, these may be outliers in the *Winterbourne et al.* [2014] compilation due to high corrections for sediment thicknesses. Discrepancies between predicted dynamic topography and estimates of residual topography could also reflect that sources of buoyancy and lateral viscosity variations are ignored in the top 350 km of the mantle in the calculation of dynamic topography, although the shallow mantle is expected to be a source of short-wavelength dynamic topography [*Colli et al.*, 2016; *Hoggard et al.*, 2016]. The match between residual and dynamic topography is comparatively better for Case 2 than the other models, with an RMS value of ~249 m and 72% of residual topography values in overall agreement with the dynamic topography prediction. The better match to residual topography in Case 2 is largely due to the lower amplitude of the predicted dynamic topography, in which the model has a viscosity jump of 100 from the upper to lower mantle (Figure 7). Although the other cases predict higher dynamic topography amplitudes, the regional and time-dependent trends (see section 3.2) that are the key to our interpretations are consistent between models.

The predicted present-day mantle temperature is qualitatively compared to *P* and *S* wave seismic tomographic models, assuming that seismic velocity anomalies largely result from thermal perturbations [*Becker and Boschi*, 2002; *Grand*, 2002]. The tomographic models share first-order similarities, but differ on scales smaller than several hundred kilometers. This is due to the earthquake sources used, earthquake relocations

applied, the crustal correction, and model parameterization [*Grand*, 2002; *Romanowicz*, 2008]. Although the *P* wave models result in higher-resolution imaging of subduction zones and the mantle beneath continents, their resolution and coverage of mantle beneath oceanic regions is more limited than *S* wave models [*Romanowicz*, 2003, 2008]. The Sunda slab has been consistently interpreted as a north-dipping feature to a depth of ~1500 km in the mantle beneath the Sundaland continental promontory in *P* wave tomography models [*Widiyantoro and van der Hilst*, 1996]. Other post-Jurassic Tethyan slabs related to subduction at the Sunda margin are beneath oceanic regions that are likely best-sampled by *S* wave tomographic models.

The highest-resolution models for the area are the *P* wave models, including MIT-P [*Li et al*., 2008] and GAP_P4 [*Obayashi et al*., 2013] (Figure 10b-10c); these models are supplemented by *S* wave models that provide more uniform sampling of the lower mantle [*Romanowicz*, 2003], including S40RTS [*Ritsema et al*., 2010] and GRAND-S [*Grand*, 2002] (Figure 10d-10e). Our numerical models (Cases 1–4) are compatible with the first-order mantle structure interpreted from *P* and *S* wave tomography (Figure 10), including the positions of the upper to mid-mantle Sunda slab and the lower mantle Meso-Tethyan and East Asian slabs (Figure 10). Importantly, the Late Cretaceous subduction hiatus along southern Sundaland reproduces the gaps in the slab at the expected depths including the mid mantle (~1500 km) and lower mantle (~2000 km, Figure 10) in Cases 2 and 4. Case 2 predicts the correct depth of the Sunda slab, and better matches residual topography than the other cases. We note that all our cases predict the Sunda slab using a range of mantle viscosity profiles and alternative absolute plate motion models. Although an assumption of vertical slab sinking would infer that the lower mantle slab material is purely from the Jurassic-Cretaceous Sundaland active margin, our time-dependent mantle flow models suggest that slabs are both from Tethyan and East Asian subduction (Figure 8).

3.2. Comparison Between Time-Dependent Predictions and the Geological Record

The Mesozoic flooding history of Southeast Asia is characterized by episodes of advancing and retreating shallow seas (Figure 11a). The regional sedimentary record is a key constraint indicating past regional flooding, such as the mid Cretaceous Eromanga and Surat basins of eastern Australia, and is therefore crucial for interpreting the dynamic topography from mantle flow models [*Gurnis et al*., 1998]. Mantle flow models show a regional prevalence of negative dynamic topography associated with Tethyan subduction along the southern Sundaland margin, and Izanagi and (proto-) Pacific subduction to the north and east (Figure 8). However, following suturing of the Woyla terranes and the West Sulawesi-East Java continental blocks to Sundaland between ~80 and 75 Ma [*Clements and Hall*, 2011; *Zahirovic et al*., 2014], the region experienced broad dynamic uplift as a consequence of subduction cessation (Figures 8 and 11b). The magmatic gap from ~75 to 61 Ma on Sumatra [*McCourt et al*., 1996] is consistent with Woyla accretion and subduction cessation, while the resumption of arc volcanism by ~60 Ma indicates renewed subduction along the entire Sundaland southern margin. Regional dynamic subsidence was reestablished from ~40 Ma (Figures 8, 11b, and 12), as negatively buoyant slabs sank in the upper mantle. This ~20 Myr lag time between subduction initiation and the development of a widespread dynamic topographic low on Sundaland is caused by the time taken for the upper mantle to be populated with sinking slabs from circum-Sundaland subduction. Although the absolute values for dynamic topography are sensitive to

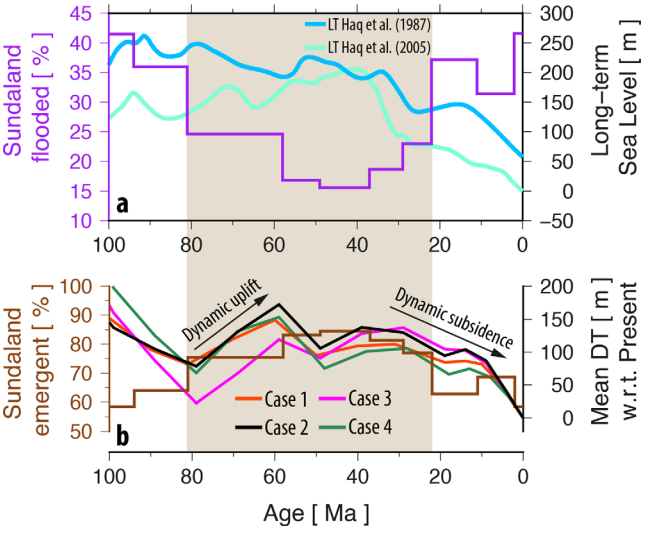

Figure 11. Processes influencing the continental inundation of Sundaland. (a) The evolution of long-term sea level (light and dark blue) with respect to present-day does not reproduce the flooding history of Sundaland. (b) The trends from regionally-averaged dynamic topography with respect to present-day (Cases 1–4) indicate a link between the emergence and flooding history of Sundaland since the Late Cretaceous, in contrast to the eustatic trends. The light brown shading in the background denotes widespread regional erosional environments likely responsible for the missing sections of rock from sedimentary sequences (Figure 3).

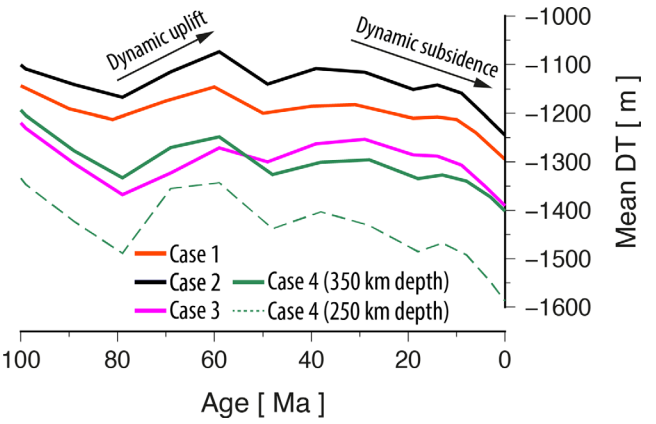

Figure 12. Mean dynamic topography (DT). Average dynamic topography for Sundaland through time in Cases 1–4 derived from sources of buoyancy deeper than 350 km (thick lines). For Case 4, we also computed the dynamic topography from sources of buoyancy deeper than 250 km (dashed thin green line), which highlights a higher amplitude of the dynamic topography prediction, while maintaining the key trends of dynamic uplift between ~80 and 60 Ma and dynamic subsidence since ~40 Ma. The thick lines are shifted in Figure 11b for the purpose of comparing trends in the dynamic topography acting on Sundaland.

the radial viscosity structure (Figure 12), and to a lesser extent the absolute plate motion reference frame, the regionally averaged dynamic topography trends are common to all models, which highlights the control of the subduction history on the dynamic topography trends for Sundaland (Figure 11b). We compute the dynamic topography considering sources of buoyancy deeper than 250 km (Figure 12, dashed green line), to verify that the timing of dynamic uplift and subsidence for Sundaland remain consistent with the dynamic topography derived from sources of buoyancy deeper than 350 km.

4. Discussion

The mantle beneath Southeast Asia has been dominated by post-Pangea subduction with long-term convergence between Eurasian, Indo-Australian, and Pacific plates. Seismic tomography of the mantle provides crucial clues in untangling the complex history of plate motions that led to the present-day labyrinthine network of suture zones and plate boundaries in Southeast Asia [*Hall and Spakman*, 2015; *Wu et al*., 2016]. By comparing plate reconstructions in a Siberia-fixed reference frame with depth slices of *P* wave seismic tomography, *Replumaz et al*. [2004] interpreted the nature and timing of key changes in the geodynamic evolution of Southeast Asia, and inferred links between surface tectonics and mantle evolution. Their interpretations suggested an average slab sinking rate of 5 and 2 cm/yr in the upper and lower mantle, respectively, and the onset of India-Eurasia continental collision at ~55–40 Ma. The dip of the Sunda slab beneath Sundaland is interpreted by *Replumaz et al*. [2004] to result from ~5–10° southward slab rollback since ~50 Ma, however, the assumed plate reconstructions in *Replumaz et al*. [2004] do not model the south-dipping subduction of the Proto South China Sea along northern Borneo since ~50 Ma [*Hutchison*, 1996; *Soeria-Atmadja et al*., 1999; *Zahirovic et al*., 2014] and do not accommodate oroclinal bending of Sundaland [*Hutchison*, 2010; *Zahirovic et al*., 2014]. The oroclinal bending was likely responsible for the ~50° counter-clockwise rotation of Borneo since 25 Ma [*Fuller et al*., 1999], which influenced the evolution of the Sunda Trench, while the subduction of the Proto South China Sea is an additional factor required in interpreting the present-day Sunda slab structure.

The work of *Kárason* [2002] applied a similar approach and interpretation as *Replumaz et al*. [2004] and modeled the evolution of the Sunda slab using an analytical Stokes flow solution using a swarm of "slablets" in a regional framework where the time-dependent position of the southward-retreating Sunda Trench was applied in the surface boundary condition. The prediction of the slab structure was filtered using synthetic seismic tomography, providing a better comparison between predicted slab structure and tomography. Our approach is somewhat similar to the time-dependent incorporation of the subduction zone location on the surface as in the model in *Kárason* [2002], but differs significantly in the modeling approach. First, the analytical solution in *Kárason* [2002] does not take into account temperature-dependence of viscosity and does not solve the energy equation. Second, the model of *Kárason* [2002] is regional and begins with a pristine mantle at ~50 Ma, and third, such an approach does not incorporate variable convergence rates or lithospheric thickness of the downgoing plate. In contrast, our global geodynamic models incorporate more realistic mantle and slab rheologies and allow us to track the origin and trajectory of slabs in the mantle. However, the work of *Kárason* [2002] presented an important development in linking tectonic reconstructions of Southeast Asia to mantle evolution and the present-day mantle structure from seismic tomography.

Sundaland's post-Jurassic long-wavelength topography has been influenced by the evolution of regional subduction zones in addition to the effect of changing global sea levels. Long-term global sea level change

plays a significant role in the advance and retreat of marine environments across continental shelves [*Gurnis*, 1993; *Haq et al*., 1987] and is therefore an important driving mechanism to consider for the flooding and emergence of Sundaland. However, our results suggest that dynamic topography played an important role in the long-term emergence and inundation of Sundaland since the Late Cretaceous. Our analysis is based on long-term sea level chronologies derived from sea level highstands (Figure 11a), representing the first and second-order sea level cycles (several to many millions of years) related to large-scale tectonics [*Lovell*, 2010; *Vail et al*., 1977], which are applicable to the long-term paleogeographic analysis of Sundaland flooding. Although a number of eustatic sea level curves exist, we favor sea level histories derived globally [*Spasojevic and Gurnis*, 2012] rather than locally because global estimates of sea level are not strongly influenced by regionally transient dynamic topography [*Conrad and Husson*, 2009; *Moucha et al*., 2008; *Müller et al*., 2008; *Spasojevic and Gurnis*, 2012]. For example, the long-term relative sea level curve derived from the Arabian Platform in *Haq and Al-Qahtani* [2005] shares major trends with the eustatic sea level curve from *Haq et al*. [1987] (Figure 11a), but shows the potential role of regional factors (including dynamic topography) that cause such regional curves to deviate from global trends.

The flooding of Sundaland between ~100 and 80 Ma is likely due to high eustatic sea levels [*Haq*, 2014; *Haq et al*., 1987] amplified by dynamic subsidence from post-Jurassic subduction [*McCourt et al*., 1996; *Zahirovic et al*., 2014]. However, the predicted dynamic topography trends alone reproduce the timing of shallow sea retreat from ~80 to 60 Ma, as well as the subsequent flooding from ~40 Ma (Figure 11b). This is in contrast with the long-term sea level trend, which is largely falling since ~30 Ma and is out of phase with the inundation of Sundaland. Thus, regional dynamic uplift during Late Cretaceous to Eocene times is a plausible mechanism for Sundaland emergence and the establishment of a contemporaneous regional unconformity. Renewed dynamic subsidence from ~40 Ma, along with the onset of rifting in many Sundaland basins, plays an important role in the long-term advance of shallow seas on the Sunda Shelf while rapidly falling global sea levels from ~15 Ma partly offset this flooding and result in widespread regressive deltaic sedimentation from mid-Miocene times [*Doust and Sumner*, 2007] (Figures 3 and 4).

In addition, the interaction of the Wharton Ridge with the Sunda active margin (Figure 4), and the resulting slab window [*Whittaker et al*., 2007], may play a role in moderating the subduction-induced dynamic subsidence. In our plate reconstructions the Wharton Ridge sweeps progressively westward across the Sunda active margin from ~60 Ma near Java until it is abandoned at ~40 Ma adjacent to Sumatra. The proximity of the Wharton Ridge at ~60–55 Ma to eastern Sundaland is contemporaneous with the onset of rifting in the Barito and Lombok basins along eastern Sundaland, with a generally westward progression of basin rift activation in Sundaland (Figure 4, Animation S1). This pattern of basin activations is consistent with oroclinal bending of Sundaland [*Hutchison*, 2010; *Zahirovic et al*., 2014], with a potential role of thermal weakening of Sundaland lithosphere and crust from a Wharton Ridge slab window. However, the geodynamic models only predict a moderating effect of the Wharton Ridge on dynamic topography, with slightly weaker dynamic subsidence for central and eastern Sundaland at ~48 Ma (Figure 8d). Our numerical experiments of mantle flow are subduction-driven, and since plumes are suppressed, the resulting dynamic topography only represents the influence of sinking slabs in the mantle and the large-scale mantle upwellings elsewhere. As a result, the subduction history dominates the dynamic topography acting on Sundaland in our models, with second order effects such as the Wharton Ridge slab window moderating the amplitude of the long-wavelength topography.

The timeframe of the regional unconformity likely represents an extended period of erosion or nondeposition, with any eroded sediments likely deposited in the Eocene-Miocene Crocker Fan on northern Borneo [*Clements and Hall*, 2007; *Clements and Hall*, 2011], where the largest volume of Paleogene sediments of Southeast Asian origin have been preserved in a single basin (Figure 2). The zircon age-spectra from the sediments confirm a distal Sundaland source, including the Cretaceous-age Schwaner (southwest Borneo) and the Permo-Triassic (Malay-Thai) Tin Belt granitoids [*van Hattum et al*., 2006], which were eroded during the Late Cretaceous to Eocene regional dynamic uplift. To the south, reworked pre-Cenozoic sediments, including sediments sourced from Southwest Borneo, were shed into a prograding deltaic system along Java to form the Ciemas and Bayah Formations (Figure 2) during the Eocene [*Clements and Hall*, 2007]. The Late Cretaceous to Eocene unconformity (Figure 3) on Sundaland itself provides no clues for the onset of the erosional event, while the resumption of Eocene-Oligocene sedimentation records post-Eocene rifting in the Gulf of Thailand, Natuna Basins, and Java Sea [*Doust and Sumner*, 2007] during which subsidence was

enhanced by stronger negative dynamic topography. Our plate reconstructions linked to numerical mantle flow models suggest that dynamic uplift started in the Late Cretaceous, sometime between ~80 and 60 Ma, based on a hiatus in subduction-related volcanism on Sumatra, Java, and Borneo [*Clements and Hall*, 2011; *McCourt et al*., 1996; *Zahirovic et al*., 2014]. Although our approach does not capture the dynamics of slab breakoff, we expect that a ~15 to 20 Myr interruption in subduction would have resulted in dynamic uplift in the overriding plate, as occurs in our models. However, since our computation of dynamic topography excludes the contributions of the shallowest ~350 km mantle depths, our modeling does not capture the full response of the crust and lithosphere to slab breakoff. Our results are therefore only relevant for the influence of large-scale mantle flow for Sundaland, and more work is required to isolate the role of crustal, lithospheric, and shallow-mantle processes during slab breakoff.

The method presented in this study uses a rigid plate motion model for Southeast Asia, with only implied continental deformations, such as the extrusion of Indochina and the oroclinal bending of Borneo [*Zahirovic et al*., 2014]. Recent work has used this rigid plate motion model as a starting point in constructing a deforming plate reconstruction for Sundaland [*Yang et al*., 2016]. The deforming plate reconstruction is incorporated into a backward advection model for the last 50 Myr (approx. Eocene), with the present-day mantle structure taken from the RUM slab model [*Gudmundsson and Sambridge*, 1998] and seismic tomography from S40RTS [*Ritsema et al*., 2011]. The backward advection method applied by *Yang et al*. [2016] also reports dynamic subsidence since the Eocene resulting from a slab avalanche, with a larger prediction of subsidence of up to ~400 m since ~40 Ma. In addition, they suggest that basin subsidence and contemporaneous basin inversion can result from an avalanching Sunda slab. Since the amplitude of past dynamic topography is difficult to constrain, we focus on the trends (Figure 11b) rather than the absolute values (Figure 12), as the trends highlight major changes in the regional dynamic uplift or subsidence. The benefit of backward advection models is that they incorporate the present-day mantle structure from seismic tomography as an initial condition, contrary to our models that are agnostic of the present-day mantle structure. However, since backward advection techniques are limited to the last ~75 Ma [*Bunge et al*., 2003; *Conrad and Gurnis*, 2003], we apply a forward modeling approach to study the longer-term evolution of dynamic topography for Southeast Asia. Future work should focus on coupling mantle flow with lithospheric and crustal-scale deformation and surface process models to better quantify the relative contributions from mantle, lithosphere, crustal, surface, and eustatic mechanisms.

5. Conclusions

A Late Cretaceous collision of Gondwana-derived terranes [*Clements et al*., 2011; *Zahirovic et al*., 2014] resulted in regional dynamic uplift and emergence due to a ~10–15 million year long subduction hiatus along the Sunda active margin [*McCourt et al*., 1996]. Regional dynamic uplift can account for the absence of sediment deposition across Sundaland and the emergence of Sundaland between ~80 and 60 Ma. Renewed subduction from ~60 Ma reinitiated dynamic subsidence of Sundaland, amplified by active rifting in a number of basins, leading to submergence from ~40 Ma despite decreasing long-term global sea levels [*Haq and Al-Qahtani*, 2005; *Haq et al*., 1987; *Spasojevic and Gurnis*, 2012]. Our results show that Sundaland experienced a complete "down-up-down" dynamic topography cycle over the last 100 million years, with the transience of topography revealed in sedimentary basin stratigraphy punctuated with regional unconformities; our explicit connection to observations is consistent with the theoretical prediction of *Burgess and Gurnis* [1995] that dynamic topography should contribute to generating unconformities over long periods of geological time. Subduction-driven mantle convection models can be useful in interpreting the geological record of basins, with major regional trends providing insights into episodes of dynamic uplift and subsidence, and thus enabling a deeper understanding of the driving forces of Earth's ephemeral coastlines.

By comparing geological data and global sea level evolution with predictions of 4-D global mantle flow models, we show that the subduction history had a strong influence over the long-term flooding and emergence of Southeast Asia on geological timescales. Our model may explain the timing of the Late Cretaceous-Eocene major regional unconformity on Sundaland, and may also account for the present-day distribution of residual topography and mantle structure. Our results capture an entire cycle of dynamic uplift and subsidence that caused an advance, retreat, and readvance of shallow marine environments on Sundaland. This process may apply to other continental regions that have experienced punctuated

episodes of subduction. Predictions of the long-term evolution of long-wavelength topography could be coupled with surface process models to understand how erosion links low-amplitude and long-wavelength dynamic uplift to regional unconformities [*Braun et al*., 2013; *Burgess and Gurnis*, 1995; *Clements et al*., 2011] and associated pulses of deposition in sedimentary basins. More generally, there is a need for methods to assess the dynamic contribution to regional sea level curves, as well as a need for new methods in linking mantle and surface processes across wide spatial and temporal scales.

Acknowledgments

S.Z. was supported by an Australian Postgraduate Award, a University of Sydney Vice Chancellor's Research Scholarship and ARC grant IH130200012. N.F. was supported by ARC IH130200012. R.D.M. and M.S. were supported by ARC grants FL0992245 and FT130101564, respectively. M.G. was partially supported by Statoil ASA and by the National Science Foundation under grants CMMI-1028978, EAR-1161046, and EAR-1247022. We thank Sierd Cloetingh, Xi Liu, and Laurent Husson for constructive reviews that helped improve the manuscript. Figures were constructed using Generic Mapping Tools [*Wessel and Smith*, 1998; *Wessel et al*., 2013], GPlates (www.gplates.org) [*Boyden et al*., 2011], TimeScale Creator, and ArcGIS. Numerical models were carried out on the Sun Constellation VAYU cluster of the Australian National Computational Infrastructure. The original *CitcomS* software was obtained from CIG, Computational Infrastructure for Geodynamics (http://geodynamics.org). We thank J. Golonka and M. Pubellier for discussions on regional and global paleogeographic and plate reconstructions. The data used are listed in the references, tables, supplements and file repository at ftp://ftp.earthbyte.org/Data_Collections/Zahirovic_etal_Sundaland_DynamicTopography.zip and ftp://ftp.earthbyte.org/Data_Collections/Muller_etal_2016_AREPS/Muller_etal_AREPS_Supplement.zip.

References

Becker, T., and L. Boschi (2002), A comparison of tomographic and geodynamic mantle models, *Geochem. Geophys. Geosyst.*, *3*(1), 1003, doi:10.1029/2001GC000168.

Bertelloni, C. L., and M. Gurnis (1997), Cenozoic subsidence and uplift of continents from time-varying dynamic topography, *Geology*, *25*(8), 735–738.

Bower, D. J., M. Gurnis, and N. Flament (2015), Assimilating lithosphere and slab history in 4-D Earth models, *Phys. Earth Planet. Inter.*, *238*, 8–22, doi:10.1016/j.pepi.2014.10.013.

Boyden, J., R. Müller, M. Gurnis, T. Torsvik, J. Clark, M. Turner, H. Ivey-Law, R. Watson, and J. Cannon (2011), Next-generation plate-tectonic reconstructions using GPlates, in *Geoinformatics: Cyberinfrastructure for the Solid Earth Sciences*, edited by G. Keller and C. Baru, pp. 95–114, Cambridge Univ. Press, Cambridge, U. K.

Braun, J., X. Robert, and T. Simon-Labric (2013), Eroding dynamic topography, *Geophys. Res. Lett.*, *40*, 1494–1499, doi:10.1002/grl.50310.

Buiter, S. J. H., R. Govers, and M. J. R. Wortel (2002), Two-dimensional simulations of surface deformation caused by slab detachment, *Tectonophysics*, *354*(3–4), 195–210, doi:10.1016/S0040-1951(02)00336-0.

Bunge, H.-P., C. Hagelberg, and B. Travis (2003), Mantle circulation models with variational data assimilation: Inferring past mantle flow and structure from plate motion histories and seismic tomography, *Geophys. J. Int.*, *152*(2), 280–301.

Burgess, P. M., and M. Gurnis (1995), Mechanisms for the formation of cratonic stratigraphic sequences, *Earth Planet. Sci. Lett.*, *136*(3), 647–663, doi:10.1016/0012-821X(95)00204-P.

Clements, B., and R. Hall (2007), Cretaceous to Late Miocene stratigraphic and tectonic evolution of West Java, *Proc. Annu. Conv. Indones. Pet. Assoc.*, *31*, 1–18.

Clements, B., and R. Hall (2011), A record of continental collision and regional sediment flux for the Cretaceous and Palaeogene core of SE Asia: Implications for early Cenozoic palaeogeography, *J. Geol. Soc.*, *168*, 1187–1200, doi:10.1144/0016-76492011-004.

Clements, B., P. Burgess, R. Hall, and M. Cottam (2011), Subsidence and uplift by slab-related mantle dynamics: A driving mechanism for the Late Cretaceous and Cenozoic evolution of continental SE Asia?, *Spec. Publ. Geol. Soc. London*, *355*(1), 37–51, doi:10.1144/SP355.3.

Colli, L., S. Ghelichkhan, and H. P. Bunge (2016), On the ratio of dynamic topography and gravity anomalies in a dynamic Earth, *Geophys. Res. Lett.*, *43*, 2510–2516, doi:10.1002/2016GL067929.

Conrad, C. P., and M. Gurnis (2003), Seismic tomography, surface uplift, and the breakup of Gondwanaland: Integrating mantle convection backwards in time, *Geochem. Geophys. Geosyst.*, *4*(3), 1031, doi:10.1029/2001GC000299.

Conrad, C. P., and L. Husson (2009), Influence of dynamic topography on sea level and its rate of change, *Lithosphere*, *1*(2), 110–120.

Davies, J., and F. von Blanckenburg (1995), Slab breakoff: A model of lithosphere detachment and its test in the magmatism and deformation of collisional orogens, *Earth Planet. Sci. Lett.*, *129*(1), 85–102, doi:10.1016/0012-821X(94)00237-S.

Doust, H., and H. S. Sumner (2007), Petroleum systems in rift basins—A collective approach in Southeast Asian basins, *Pet. Geosci.*, *13*(2), 127–144, doi:10.1144/1354-079307-746.

Duretz, T., T. V. Gerya, and W. Spakman (2014), Slab detachment in laterally varying subduction zones: 3-D numerical modeling, *Geophys. Res. Lett.*, *41*, 1951–1956, doi:10.1002/2014GL059472.

Flament, N., M. Gurnis, S. E. Williams, M. Seton, J. Skogseid, C. Heine, and R. D. Müller (2014), Topographic asymmetry of the South Atlantic from global models of mantle flow and lithospheric stretching, *Earth Planet. Sci. Lett.*, *387*, 107–119, doi:10.1016/j.epsl.2013.11.017.

Fuller, M., J. R. Ali, S. J. Moss, G. M. Frost, B. Richter, and A. Mahfi (1999), Paleomagnetism of Borneo, *J. Asian Earth Sci.*, *17*(1–2), 3–24, doi:10.1016/S0743-9547(98)00057-9.

Golonka, J., M. Krobicki, J. Pajak, N. Van Giang, and W. Zuchiewicz (2006), *Global Plate Tectonics and Paleogeography of Southeast Asia*, 128 pp., Fac. of Geol., Geophys. and Environ. Prot., AGH Univ. of Sci. and Technol., Krakow, Poland.

Grand, S. (2002), Mantle shear-wave tomography and the fate of subducted slabs, *Philos. Trans. R. Soc. London A*, *360*(1800), 2475.

Gudmundsson, Ó., and M. Sambridge (1998), A regionalized upper mantle (RUM) seismic model, *J. Geophys. Res.*, *103*(B4), 7121–7136.

Gurnis, M. (1991), Continental flooding and mantle-lithosphere dynamics, in *Glacial Isostasy, Sea-Level and Mantle Rheology*, pp. 445–492, Springer Science+Business Media, Dordrecht.

Gurnis, M. (1993), Phanerozoic marine inundation of continents driven by dynamic topography above subducting slabs, *Nature*, *364*, 589–593, doi:10.1038/364589a0.

Gurnis, M., R. Müller, and L. Moresi (1998), Cretaceous vertical motion of Australia and the Australian Antarctic discordance, *Science*, *279*(5356), 1499–1504, doi:10.1126/science.279.5356.1499.

Hager, B., R. Clayton, M. Richards, R. Comer, and A. Dziewonski (1985), Lower mantle heterogeneity, dynamic topography and the geoid, *Nature*, *313*(6003), 541–545.

Hall, R. (2002), Cenozoic geological and plate tectonic evolution of SE Asia and the SW Pacific: Computer-based reconstructions, model and animations, *J. Asian Earth Sci.*, *20*(4), 353–431, doi:10.1016/S0012-821X(04)00070-6.

Hall, R., and W. Spakman (2015), Mantle structure and tectonic history of SE Asia, *Tectonophysics*, *658*, 14–45, doi:10.1016/j.tecto.2015.07.003.

Haq, B. U. (2014), Cretaceous eustasy revisited, *Global Planet. Change*, *113*, 44–58, doi:10.1016/j.gloplacha.2013.12.007.

Haq, B. U., and A. M. Al-Qahtani (2005), Phanerozoic cycles of sea-level change on the Arabian Platform, *GeoArabia*, *10*(2), 127–160.

Haq, B. U., J. Hardenbol, and P. R. Vail (1987), Chronology of fluctuating sea levels since the Triassic, *Science*, *235*(4793), 1156–1167, doi:10.1126/science.235.4793.1156.

Hoggard, M., N. White, and D. Al-Attar (2016), Global dynamic topography observations reveal limited influence of large-scale mantle flow, *Nat. Geosci.*, *9*, 456–463.

Hutchison, C. S. (1975), Ophiolite in Southeast Asia, *Geol. Soc. Am. Bull.*, *86*(6), 797–806, doi:10.1130/0016-7606(1975)86<797:OISA>2.0.CO;2.

Hutchison, C. S. (1996), The 'Rajang accretionary prism' and 'Lupar Line' problem of Borneo, *Spec. Publ. Geol. Soc. London*, *106*(1), 247–261, doi:10.1144/GSL.SP.1996.106.01.16.
Hutchison, C. S. (2010), Oroclines and paleomagnetism in Borneo and South-East Asia, *Tectonophysics*, *496*(1), 53–67, doi:10.1016/j.tecto.2010.10.008.
Kárason, H. (2002), Constraints on mantle convection from seismic tomography and flow modeling, PhD thesis, Mass. Inst. of Technol., Cambridge.
Katili, J. A. (1975), Volcanism and plate tectonics in the Indonesian island arcs, *Tectonophysics*, *26*(3), 165–188, doi:10.1016/0040-1951(75)90088-8.
Lee, T.-Y., and L. A. Lawver (1995), Cenozoic plate reconstruction of Southeast Asia, *Tectonophysics*, *251*(1–4), 85–138, doi:10.1016/0040-1951(95)00023-2.
Li, C., R. van der Hilst, E. Engdahl, and S. Burdick (2008), A new global model for P wave speed variations in Earth's mantle, *Geochem. Geophys. Geosyst.*, *9*, Q05018, doi:10.1029/2007GC001806.
Li, Z. H., Z. Xu, T. Gerya, and J.-P. Burg (2013), Collision of continental corner from 3-D numerical modeling, *Earth Planet. Sci. Lett.*, *380*, 98–111.
Lovell, B. (2010), A pulse in the planet: Regional control of high-frequency changes in relative sea level by mantle convection, *J. Geol. Soc.*, *167*(4), 637–648, doi:10.1144/0016-76492009-127.
McCourt, W., M. Crow, E. Cobbing, and T. Amin (1996), Mesozoic and Cenozoic plutonic evolution of SE Asia: Evidence from Sumatra, Indonesia, *Spec. Publ. Geol. Soc. London*, *106*(1), 321–335, doi:10.1144/GSL.SP.1996.106.01.21.
McKenzie, D. (2010), The influence of dynamically supported topography on estimates of Te, *Earth Planet. Sci. Lett.*, *295*(1), 127–138, doi:10.1016/j.epsl.2010.03.033.
Metcalfe, I. (1988), Origin and assembly of south-east Asian continental terranes, *Spec. Publ. Geol. Soc. London*, *37*(1), 101–118, doi:10.1144/GSL.SP.1988.037.01.08.
Moucha, R., A. M. Forte, J. X. Mitrovica, D. B. Rowley, S. Quéré, N. A. Simmons, and S. P. Grand (2008), Dynamic topography and long-term sea-level variations: There is no such thing as a stable continental platform, *Earth Planet. Sci. Lett.*, *271*(1), 101–108, doi:10.1016/j.epsl.2008.03.056.
Müller, R., M. Sdrolias, C. Gaina, B. Steinberger, and C. Heine (2008), Long-term sea-level fluctuations driven by ocean basin dynamics, *Science*, *319*(5868), 1357.
Müller, R. D., et al. (2016), Ocean basin evolution and global-scale plate reorganization events since Pangea breakup, *Annu. Rev. Earth Planet. Sci.*, *44*, 107–138.
Obayashi, M., J. Yoshimitsu, G. Nolet, Y. Fukao, H. Shiobara, H. Sugioka, H. Miyamachi, and Y. Gao (2013), Finite frequency whole mantle P wave tomography: Improvement of subducted slab images, *Geophys. Res. Lett.*, *40*(21), 5652–5657, doi:10.1002/2013GL057401.
Replumaz, A., H. Karason, R. D. van der Hilst, J. Besse, and P. Tapponnier (2004), 4-D evolution of SE Asia's mantle from geological reconstructions and seismic tomography, *Earth Planet. Sci. Lett.*, *221*(1–4), 103–115.
Ritsema, J., A. Deuss, H. Van Heijst, and J. Woodhouse (2010), S40RTS: A degree-40 shear-velocity model for the mantle from new Rayleigh wave dispersion, teleseismic traveltime and normal-mode splitting function measurements, *Geophys. J. Int.*, *184*, 1223–1236, doi:10.1111/j.1365-246X.2010.04884.x.
Ritsema, J., A. Deuss, H. Van Heijst, and J. Woodhouse (2011), S40RTS: A degree-40 shear-velocity model for the mantle from new Rayleigh wave dispersion, teleseismic traveltime and normal-mode splitting function measurements, *Geophys. J. Int.*, *184*(3), 1223–1236.
Romanowicz, B. (2003), Global mantle tomography: Progress status in the past 10 years, *Annu. Rev. Earth Planet. Sci.*, *31*(1), 303–328.
Romanowicz, B. (2008), Using seismic waves to image Earth's internal structure, *Nature*, *451*(7176), 266–268.
Seton, M., C. Gaina, R. D. Müller, and C. Heine (2009), Mid-Cretaceous seafloor spreading pulse: Fact or fiction?, *Geology*, *37*(8), 687–690, doi:10.1130/G25624A.1.
Seton, M., et al. (2012), Global continental and ocean basin reconstructions since 200 Ma, *Earth Sci. Rev.*, *113*(3–4), 212–270, doi:10.1016/j.earscirev.2012.03.002.
Soeria-Atmadja, R., D. Noeradi, and B. Priadi (1999), Cenozoic magmatism in Kalimantan and its related geodynamic evolution, *J. Asian Earth Sci.*, *17*(1), 25–45, doi:10.1016/S0743-9547(98)00062-2.
Spasojevic, S., and M. Gurnis (2012), Sea level and vertical motion of continents from dynamic earth models since the Late Cretaceous, *AAPG Bull.*, *96*(11), 2037–2064, doi:10.1306/03261211121.
Steinberger, B., and A. R. Calderwood (2006), Models of large-scale viscous flow in the Earth's mantle with constraints from mineral physics and surface observations, *Geophys. J. Int.*, *167*(3), 1461–1481, doi:10.1111/j.1365-246X.2006.03131.x.
Steinberger, B., and T. H. Torsvik (2008), Absolute plate motions and true polar wander in the absence of hotspot tracks, *Nature*, *452*(7187), 620–623, doi:10.1038/nature06824.
Torsvik, T., R. Müller, R. Van der Voo, B. Steinberger, and C. Gaina (2008), Global plate motion frames: Toward a unified model, *Rev. Geophys.*, *46*, RG3004, doi:10.1029/2007RG000227.
Vail, P. R., R. Mitchum Jr, and S. Thompson III (1977), Seismic stratigraphy and global changes of sea level: Part 4. Global cycles of relative changes of sea level: Section 2. Application of seismic reflection configuration to stratigraphic interpretation, in *Seismic Stratigraphy—Applications to Hydrocarbon Exploration, AAPG Mem*. 26, edited by C. E. Payton, pp. 63–81.
van der Meer, D. G., W. Spakman, D. J. van Hinsbergen, M. L. Amaru, and T. H. Torsvik (2010), Towards absolute plate motions constrained by lower-mantle slab remnants, *Nat. Geosci.*, *3*(1), 36–40, doi:10.1038/ngeo708.
van Hattum, M. W., R. Hall, A. L. Pickard, and G. J. Nichols (2006), Southeast Asian sediments not from Asia: Provenance and geochronology of north Borneo sandstones, *Geology*, *34*(7), 589–592, doi:10.1130/G21939.1.
van Hunen, J., and M. B. Allen (2011), Continental collision and slab break-off: A comparison of 3-D numerical models with observations, *Earth Planet. Sci. Lett.*, *302*(1), 27–37.
Wessel, P., and W. H. Smith (1998), New, improved version of Generic Mapping Tools released, *Eos Trans. AGU*, *79*(47), 579–579, doi:10.1029/98EO00426.
Wessel, P., W. H. Smith, R. Scharroo, J. Luis, and F. Wobbe (2013), Generic Mapping Tools: Improved version released, *Eos Trans. AGU*, *94*(45), 409–410, doi:10.1002/2013EO450001.
Whittaker, J., R. Müller, M. Sdrolias, and C. Heine (2007), Sunda-Java trench kinematics, slab window formation and overriding plate deformation since the Cretaceous, *Earth Planet. Sci. Lett.*, *255*(3), 445–457, doi:10.1016/j.epsl.2006.12.031.
Widiyantoro, S., and R. D. van der Hilst (1996), Structure and evolution of subducted lithosphere beneath the Sunda arc, Indonesia, *Sci. Rep.*, *271*(5255), 1566–1570.
Wilson, M. E., and S. J. Moss (1999), Cenozoic palaeogeographic evolution of Sulawesi and Borneo, *Palaeogeography, Palaeoclimatology, Palaeoecology*, *145*(4), 303–337.

Winterbourne, J., N. White, and A. Crosby (2014), Accurate measurements of residual topography from the oceanic realm, *Tectonics*, *33*, 982–1015, doi:10.1002/2013TC003372.

Wright, N., S. Zahirovic, R. D. Müller, and M. Seton (2013), Towards community-driven paleogeographic reconstructions: Integrating open-access paleogeographic and paleobiology data with plate tectonics, *Biogeosciences*, *10*(3), 1529–1541, doi:10.5194/bg-10-1529-2013.

Wu, J., J. Suppe, R. Lu, and R. Kanda (2016), Philippine Sea and East Asian plate tectonics since 52 Ma constrained by new subducted slab reconstruction methods, *J. Geophys. Res. Solid Earth*, *121*, 4670–4741, doi:10.1002/2016JB012923.

Yang, T., M. Gurnis, and S. Zahirovic (2016), Mantle-induced subsidence and compression in SE Asia since the early Miocene, *Geophys. Res. Lett.*, *43*, 1901–1909, doi:10.1002/2016GL068050.

Zahirovic, S., M. Seton, and R. D. Müller (2014), The Cretaceous and Cenozoic tectonic evolution of Southeast Asia, *Solid Earth (EGU)*, *5*, 227–273, doi:10.5194/se-5-227-2014.

Zhong, S., A. McNamara, E. Tan, L. Moresi, and M. Gurnis (2008), A benchmark study on mantle convection in a 3-D spherical shell using CitcomS, *Geochem. Geophys. Geosyst.*, *9*, Q10017, doi:10.1029/2008GC002048.